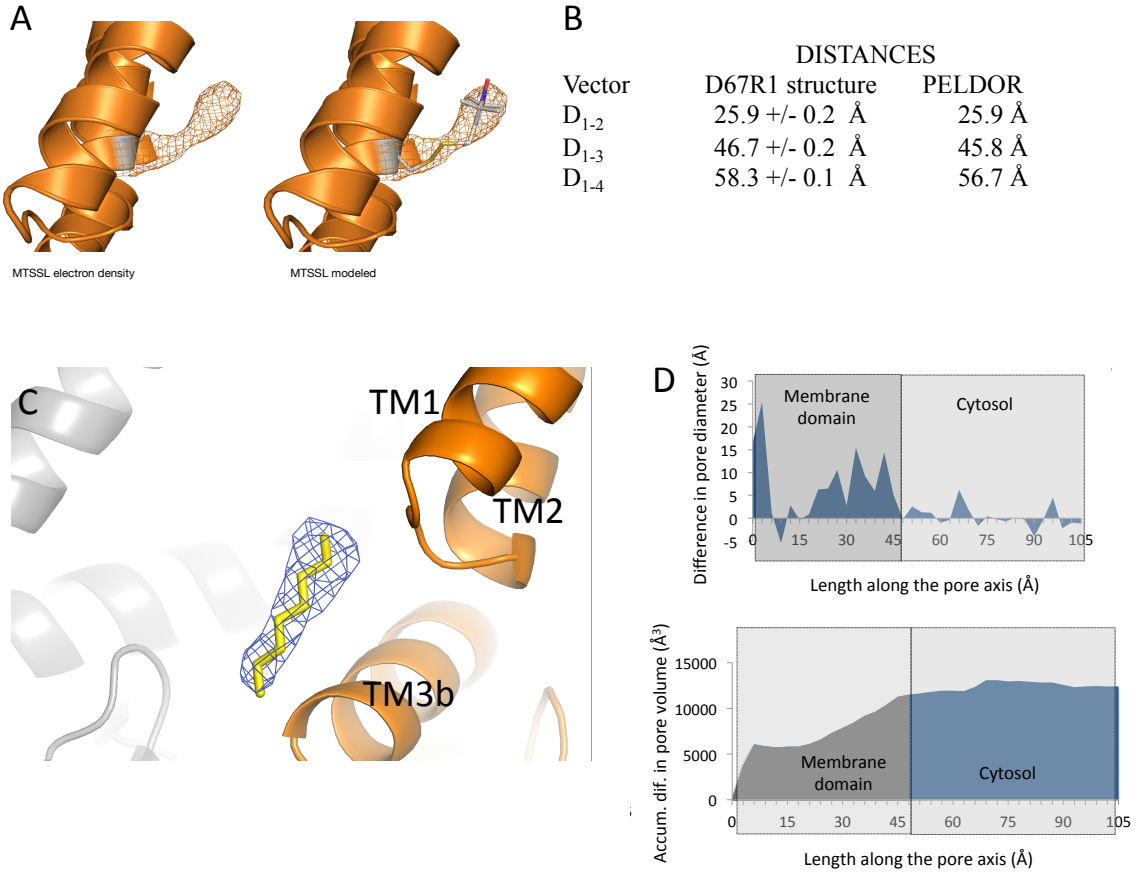

Supplementary Figure 1

Additional structural data

A: The spin label on D67R1 is clearly visible.

B: Mean spin-to-spin x-ray (measured at O of the NO group) and PELDOR distances, these are taken from the original paper[1]. The vectors are from subunit A to B (D_{1-2}), A to C, (D_{1-3}) and A to D (D_{1-4}). The D_{1-3} spin-to-spin distance (46.7 ± 0.2) Å differs only by 1Å from the PELDOR value (Fig S1B), whilst the D_{1-4} distance (58.3 ± 0.1) Å differs by 1.5 Å[1]. The increased deviation in the higher order vectors may be measurement error or be a manifestation of multispin effects[2].

C: Electron density 2Fo-Fc at 1σ for the acyl chains.

D: The internal pore diameter was measured using Porewalker software[3] in 3 Å steps starting from the resolved Y27 of the 2OAU structure (closed) and L23 of the open structure in this study with D67R1 mutated *in silico* to native. With this approach the structures have essentially the same length of 105 Å (Z-axis) using residues 23-278 (open) and 27-278 (closed). This is because the change in the tilt of the helices, means one residue in one structure is not in the same lateral plane as the same residue in the other structure. The Z-axis can be split into 35 steps along and diameter of the pore measured at each point, the pore volume can be integrated along the Z-axis. The cumulative pore volume difference of the structures for 45 Å starting at the periplasmic top of the structure along pore Z-axis (includes the whole of the TM domain) is 10,389 $Å^3$. To assess the change in pocket volumes the structures (with D67R1 again mutated *in silico* to native) were analyzed with the CASTp server[4] with probes of radii 1.5, 2.0, 2.5 and 3.0 Å. At all probe radii, the pockets in the closed structure are identified as a single volume, thus the volume of each pocket is estimated at 1/7 of this volume. The pocket volumes are 4500 $Å^3$ (3 Å probe), 5161 $Å^3$ (2.5 Å probe), 5629 $Å^3$ (2 Å probe) and 6262 $Å^3$ (1.5 Å probe); the corresponding central cavity volumes are 60,895, 62, 727, 64,965 and 68,344 $Å^3$ respectively (for the two larger probes the central cavity is split by the hydrophobic seal at L105). In the open structure analysed with a probe of 3.0 Å the central cavity is separated from the pockets with a volume of 65,276 $Å^3$ but the pockets are split into sub pockets so were not analyzed at this radius. With a probe of 2.5 Å radius, three pockets and the central cavity are considered a single volume of 78,386 $Å^3$, the remaining four pockets are identified individually, the largest and most complete was 3,892 $Å^3$. Assuming this is correct pocket would give a central cavity volume of 78,386 – 3 x 3,892 = 66,710 $Å^3$ in close agreement with the 3.0 Å probe. Thus with a 2.5 Å probe we estimate the pocket volume is reduced by 1,269 $Å^3$.

With a radius of 2.5 Å probe, all seven pockets and the central cavity are considered as one volume of 98,140 $Å^3$. To estimate the reduction in the pocket volume, we combine the volumes from the closed structure for the central cavity and pockets (64,965 + 39,403 = 104,368 $Å^3$) then substrate the volume of the seven pockets and central cavity from the open structure (98,140 $Å^3$), dividing the result by seven to yield reduction of 890 $Å^3$ in volume per pocket. This approach estimates the central cavity in the open structure as 64,967 $Å^3$ similar to the other probes. Repeating this approach with the 1.5 Å probe reveals a single volume of 107,457 $Å^3$ which using the approach detailed for the 2.0 Å probe yields a reduction in each pocket volume of 674 $Å^3$ upon opening and a central cavity of 68,343 $Å^3$. Discussion of the cross sectional area is given below.

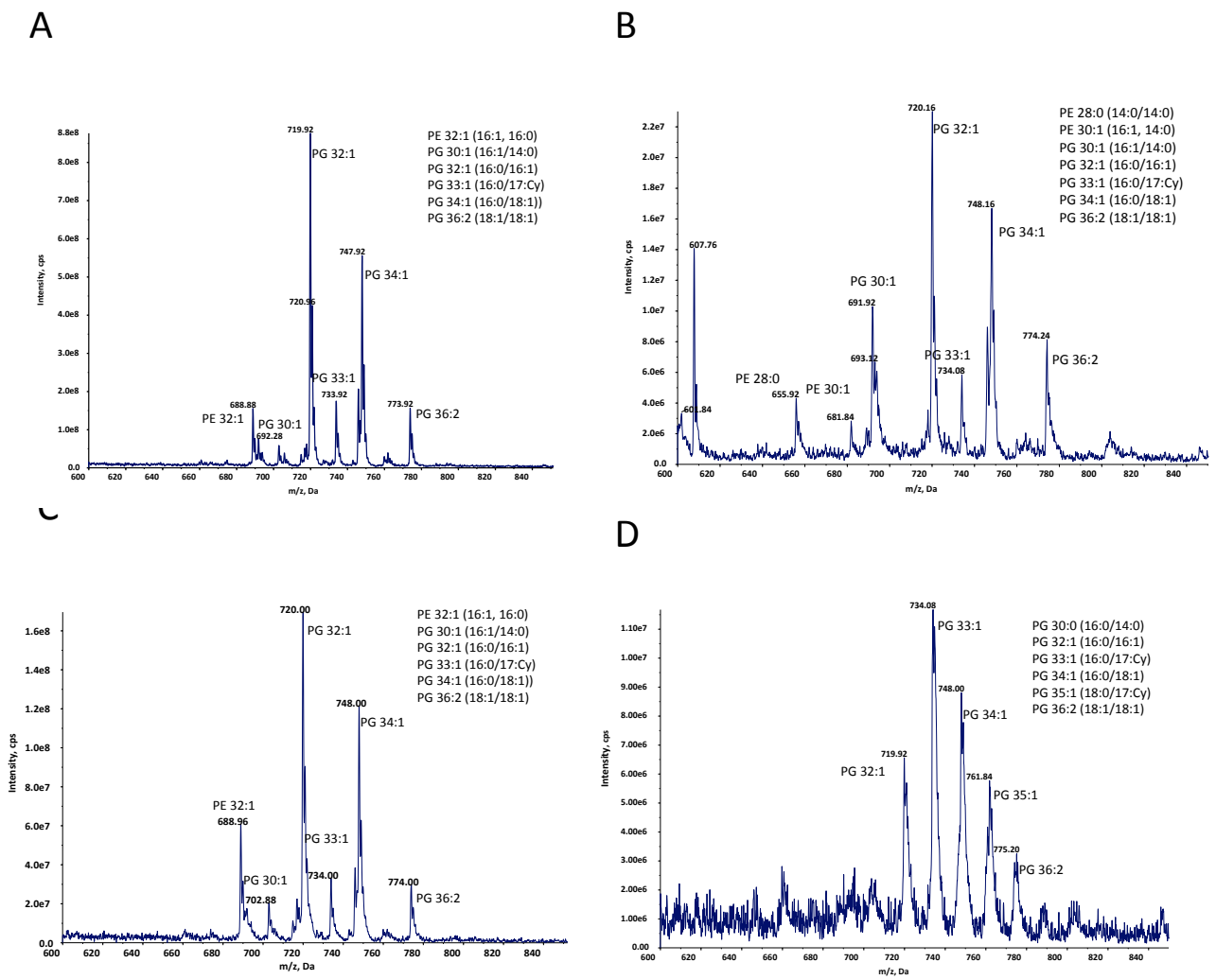

Supplementary Figure 2

Additional lipid analysis

A: Mass spectrum of the total lipid from MJF612 *E. coli* strain expressing MscS.

B: DM-solubilized MscS shows the same shift in lipid profile relative to the total lipid profile (Fig S2A) as DDM, suggesting it is not a simple property of the detergent.

C: Mass spectrum of the total lipid from MJF612 *E. coli* strain which are not expressing MscS. The lipid profile is not altered by presence or absence of MscS.

D: DDM-solubilized membrane protein (uniprot G1FG65) shows the same profile as the *E. coli* cell.

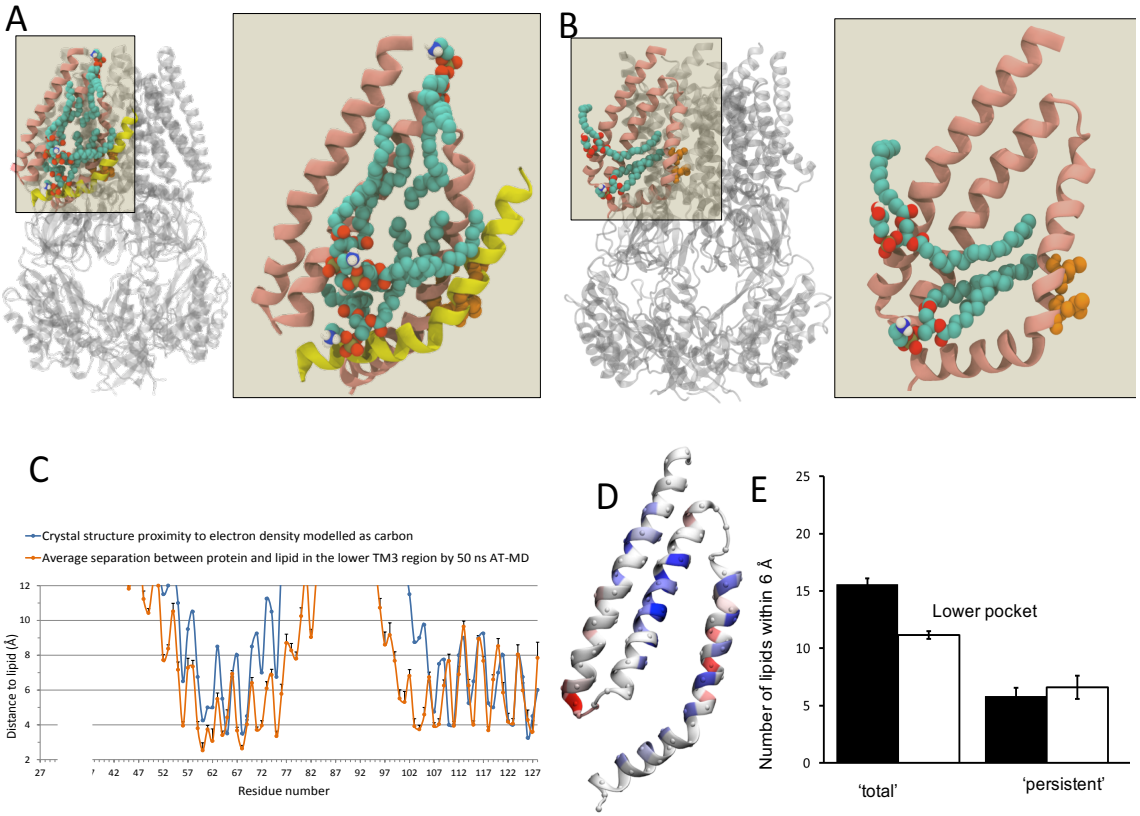
A
B
C
Crystal structure proximity to electron density modelled as carbon
Average separation between protein and lipid in the lower TM3 region by 50 ns AT-MD
Distance to lipid (Å)
Residue number
D
E
Number of lipids within 6 Å
Lower pocket
'total'
'persistent'
F
i
Strong POPE headgroup contacts to the lower TM3 region
PO4
NH3
Number of contacts (AU)
Arg 46
Ser 49
Asn 50
Asn 53
Arg 59
Lys 60
Ile 61
Asp 62
Thr 64
Asp 67
Phe 68
Ser 70
Ala 71
Arg 74
Tyr 75
Val 122
Met 126
Phe 127
Arg 128
Gln 149
Ile 150
Phe 151
Residue number and amino acid
Residue
ii
iii

Supplementary Figure 3

Additional molecular dynamics analysis.

A: Representative view of lipid interaction with a single subunit of the closed MscS structure. Full heptameric structure of closed MscS is shown. A section of the TM domain and the lipids within the pocket is enlarged to show lipid interactions with the polypeptide chain of a single monomer (salmon). The TM3ab helices of the adjacent subunit are shown in yellow, with the hydrophobic gate residues in orange (in space-filling representation). Phospholipids are shown as space-filling representations, with the colours set to distinguish the acyl tails (turquoise) from the headgroups. Note the orientation of the lipids: headgroups pointing downwards with respect to the tails signify a lipid in the cytosolic bilayer leaflet. The opposite orientation signifies a lipid in the periplasmic leaflet (c.f. Fig 3 A, B)

B: Representative view of lipid interaction with a single subunit of the open MscS structure. The heptameric structure of open MscS is shown, with a section of the TM domain and the lipids within the pocket enlarged to show lipid interactions with the polypeptide chain of a single monomer (salmon). The hydrophobic gate residues are shown in orange space-filling representations. Phospholipid representations and significance of orientation as in Fig S3A.

C: Protein proximity to lipid during AT-MD is correlated with proximity to proposed lipid in the crystal structure. Average separation between a single subunit from the new open structure and persistent lipid in the lower region of the pocket during 50-100 ns AT-MD (orange, error bars show one standard deviation) compared to the separation between the new crystal structure and electron density, modelled as carbon (blue).

D: Lipid contacts to the closed and open structures differ significantly. Data were collected from 50 to 100 ns during each AT-MD simulation, and averaged across 5 simulations per state. Statistically different numbers of lipids within 6 Å between closed and open states are shown per residue as heat-mapped residues on the polypeptide chain of the TM domain from a single subunit in the closed structure ($p < 0.01$). A dark blue residue indicates more contacts to the closed state (maximum 1.7 lipids more) whereas red indicates that the open state has more lipid contacts to the residue (maximum 1.4 lipids more). A white residue indicates no significant difference in contact number between the two states.

E: 'Persistent' (those that remain with 6 Å contact of residues in the pockets during the length simulation) and total (including those that are exchanged with the bilayer during the simulation). Dark bars are those in the closed, white in the open structure.

F: (i) The headgroups of the persisting POPE lipids shown in (iii) were analysed for contact preferences to MscS residues. Headgroups make most contacts to charges along the TM1/TM2 helices. 'Persistent' lipid configurations in the lower pocket region in the closed (ii) and open (iii) state of MscS. Lipids that make contact (6 Å cutoff) to the lower pocket region throughout 50 to 100 ns AT-MD are displayed in snapshots from the end of the respective simulations. Lipid molecules in the open structure reach the hydrophobic seal (iii), whereas the lipids in the closed structure are prevented from reaching the seal (ii).

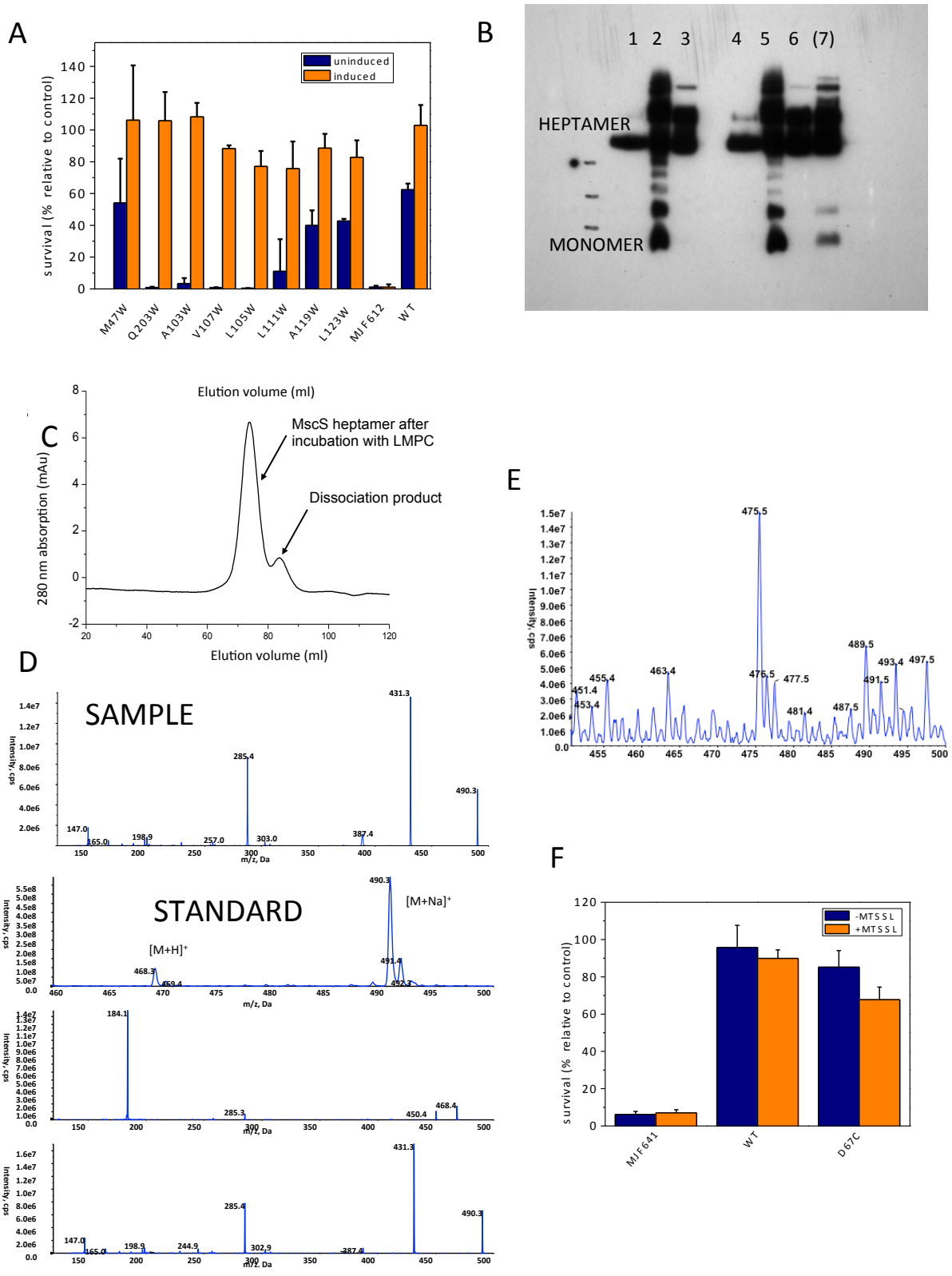

Supplementary Figure 4

Additional data on MscS mutants and effect of LPC on MscS.

A: MscS tryptophan mutants transformed into MJF612 were exposed to an osmotic downshock of 0.5 M NaCl. Samples were uninduced (blue) or induced by 0.3 mM IPTG (orange). Survival of samples are shown relative to samples diluted into control medium. All survival experiments were performed using transformants of either MJF641 (ΔyggB, ΔmscL, ΔmscK ΔybdG, ΔybiO, ΔynaI, ΔyjeP) or MJF612 (ΔyggB, ΔmscL, ΔmscK, ΔybdG). First, cells were grown at 37 °C in Luria−Bertani (LB) medium, and both induced (0.3 mM IPTG added when OD650nm ≈ 0.2) and uninduced cultures were studied. The culture was adapted to high osmolarity by growth to an OD650nm of 0.3 in the presence of 0.5 M NaCl, and an osmotic downshock was then applied by a 1:20 dilution into LB medium (shock) or the medium containing 0.5 M NaCl (control). After 10 min incubation at 37 °C, 5 μL serial dilutions of these cultures were spread onto LB-agar plates in the presence (control) or absence (shock) of 0.5 M NaCl. The survival rates were then assessed by counting the number of colonies after incubation overnight at 37 °C. Data are reported as means ± standard deviation.

B: A western blot (anti His tag), 3 second exposure of blue native gels. The lanes correspond to:

1: A119W: reconstituted in DOPC, +BrLPC, then concentrated

2: A119W: after purification in DDM, +BrLPC

3: A119W: after purification in DDM

4: M47W: reconstituted in DOPC, +BrLPC, then concentrated

5: M47W: after purification in DDM, +BrLPC

6: M47W: after purification in DDM

The data show that brominated LPC 18:1 does not dissociate the heptamer in lipid bilayers but LPC (either 18:1 or 14:0) does dissociate MscS partially in detergent (consistent with gel filtration S4B).

C: When LPC is added to detergent (not reconstituted in bilayer) solubilized MscS (mole ratio 0.3 LPC), some dissociation of the MscS heptamer is observed, we only analysed the heptameric fraction.

D: Fragmentation of the lipid extract from the heptamer confirms the identity of the lipid in Fig 1E to be LPC 14:0 to be present by comparison to LPC 14:0 standard (shown below).

E: The same control protein as used in Supplementary Fig 2D incubated with LPC 14:0 using the same protocol as MscS does not show (unlike MscS) retention of LPC 14:0 in ESI-MS/MS.

F: MscS mutants transformed into MJF641 were induced by 0.3 mM IPTG and exposed to an osmotic downshock of 0.3 M NaCl. Samples with (orange) or without (blue) addition of 0.5 mM MTSSL during the shock phase are shown.

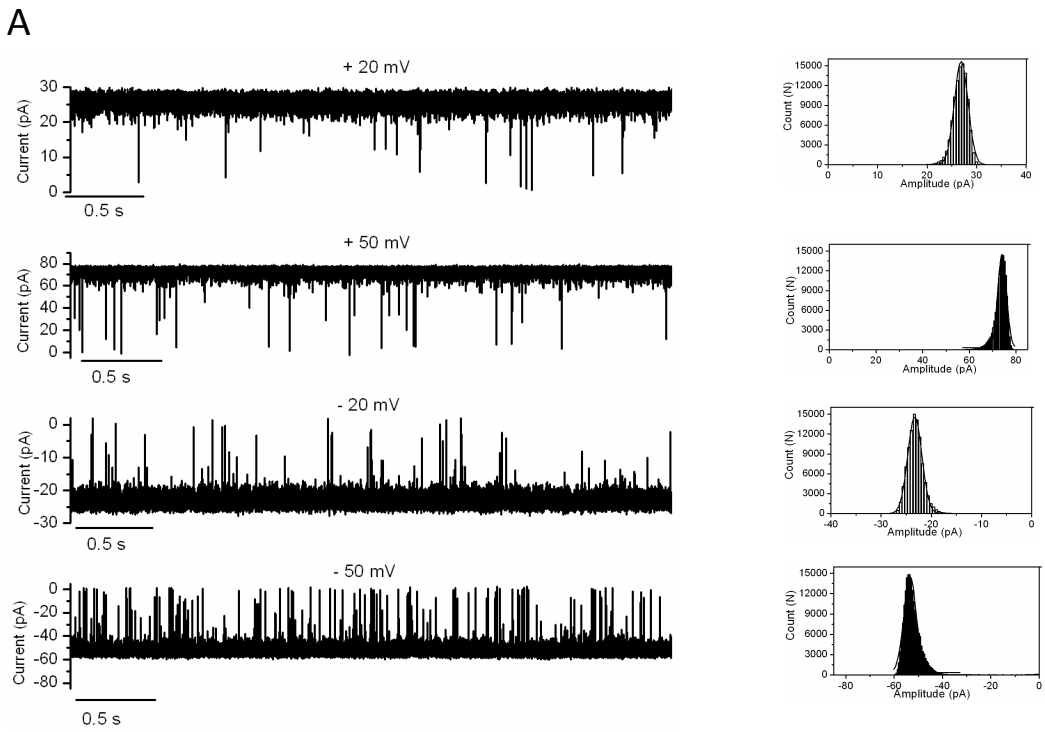
A
+ 20 mV
Current (pA)
0.5 s
Count (N)
Amplitude (pA)
+ 50 mV
- 20 mV
- 50 mV

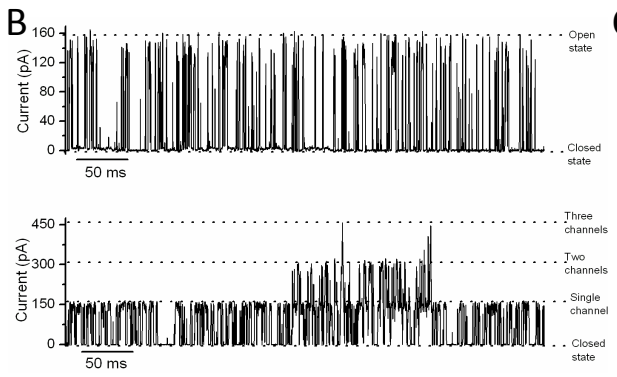
B
Current (pA)
50 ms
Open state
Closed state
Three channels
Two channels
Single channel

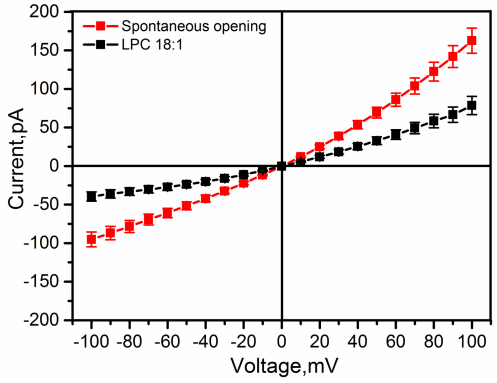
C
Spontaneous opening
LPC 18:1
Current,pA
Voltage,mV

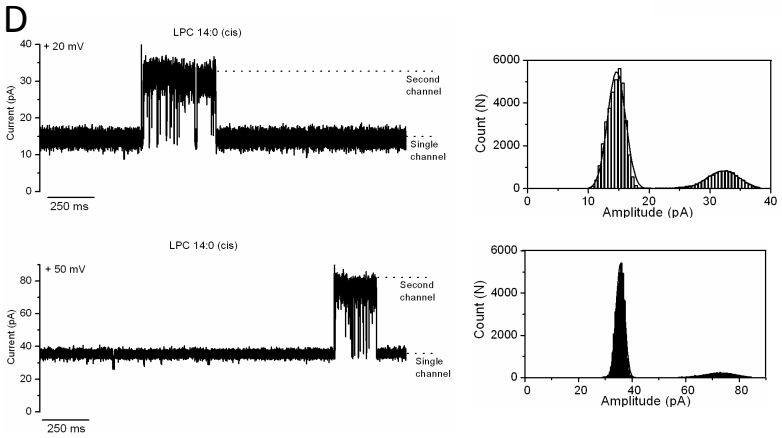
D
LPC 14:0 (cis)
+ 20 mV
Second channel
Single channel
250 ms
Count (N)
Amplitude (pA)
+ 50 mV

Supplementary Figure 5

Additional single molecule data on MscS.

A: Typical current recordings of MscS channels after spontaneous opening at +20 mV, +50 mV, -20 mV and -50 mV. All-points amplitude histograms (right panel). Electrolyte: 200 mM KCl, 90 mM $MgCl_2$, 10 mM $CaCl_2$, 10 mM HEPES, pH 7.5. 70 % spontaneously opened channel were stable with higher open probability without any closures recorded at +50 mV, -50 mV, +20 mV and -20 mV.

B: Typical current recordings at +100 mV of spontaneously opened MscS channels. Upper: gating in a single channel manifested as fast flickering. Lower: gating events in three channels. Electrolyte: 200 mM KCl, 90 mM $MgCl_2$, 10 mM $CaCl_2$, 10 mM HEPES, pH 7.5. 30 % of spontaneously opened channel showed fast flickering activity only at higher voltages +100 mV and we have not observed this fast flickering spontaneous channel opening at lower voltages (+50 mV and +20 mV). The observation of multiple channels is an important control. If the conductance arises from a single molecule, then multiple insertions should give rise to conductance that is multiples thereof. It also eliminates concerns about protein heterogeneity, that is, it is MscS, not another protein, that gives rise to the conductance data in the presence of LPC. We did not explore further the voltage dependence of spontaneous opening as this was outside the scope of the study.

C: I-V curves obtained with single MscS channels in planar lipid bilayer measured at applied potential -100 mV to 100 mV. Electrolyte: 200 mM KCl, 90 mM $MgCl_2$, 10 mM $CaCl_2$, 10 mM HEPES, pH 7.5.

D: Selected ion current recordings at + 20 mV and + 50 mV of MscS channels reconstituted into a planar lipid membrane and activated by 10 μM LPC 14:0 (cis). In both cases, the activation of a second channel with identical conductance to the first can be observed, shown as an important control. All-points amplitude histograms (right panel). Electrolyte: 200 mM KCl, 90 mM $MgCl_2$, 10 mM $CaCl_2$, 10 mM HEPES, pH 7.5. The single channel is mostly open 100% of the time with a second channel that appears to exhibit a much smaller open probability was a very rare event but importantly it demonstrated a similar conductance (thus providing a control). We do not have enough observations to determine the open probability of the ‘second’ channel and this was outwith the scope of our study.

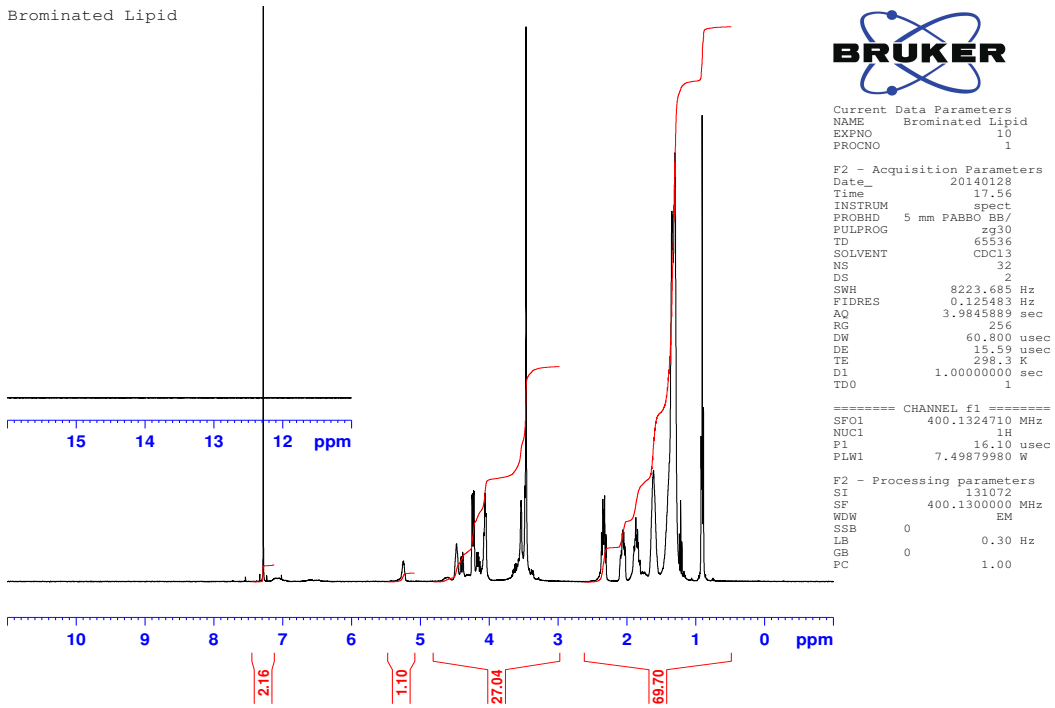

Supplementary Figure 6

Bromolipids

1H NMR spectrum of 1,2-di-(9,10-dibromo)stearoyl-sn-glycero-3-phosphocholine. The sample was solved in $CDCl_3$ and the spectrum recorded at room temperature on a 400 MHz Bruker Avance III spectrometer: $CDCl_3$): δH 0.91 (6H, m, ω-CH_3), 1.30 (40H, m, CH_2), 1.61 (7H, m, β-CH_2 and H_2O), 1.87 (5H, m, trans CH_2CHBr), 2.06 (3H, m, gauche CH_2CHBr), 2.32 (4H, m, α-CH_2), 3.47 (9H, s, $N(CH_3)_3$), 3.54 (4H, m, CHBr), 4.06 (2H, m, PO_3CH_2 (glycerol)), 4.16 (1H, m, CH_2O (glycerol)), 4.22 (2H, m, CH_2N), 4.39 (1H, m, CH_2O (glycerol)), 4.48 (2H, m, CH_2O (glycerol)), 5.24 (1H, m, CHO)[5,6]. The sample was also examined with positive ion electrospray mass spectroscopy in the presence of formic acid with an Agilent Technologies 6120 ESI-MS. Expected highest peak for $(M+H)^+$ = 1106.3 m/z (observed 1106.2 m/z). The peak pattern was as expected for an isotope cluster with four bromine atoms. The highest intensity peaks cluster in the experimental spectrum can be explained with the (M-Br) fragment. The peak pattern was as expected for an isotope cluster with three bromine atoms. Isotope clusters were simulated with the program IsoPro 3.1 (Mike Senko; https://sites.google.com/site/isoproms/).